RSC Advances

ROYAL SOCIETY OF CHEMISTRY

www.rsc.org/advances

Deactivation of Ti and Zr Half-Metallocene Complexes Activated with $B(C_6F_5)_3$: A Case Study in Constructing DFT-Based QSARs to Predict Unimolecular Rate Constants

Thomas A. Manz[a,b,c]*

[a]Department of Chemical & Materials Engineering, New Mexico State University, Las Cruces, NM 88003-8001. [b]School of Chemical Engineering, Purdue University, West Lafayette, IN 47907-2100. [c]School of Chemical & Biomolecular Engineering, Georgia Institute of Technology, Atlanta, GA 30332-0100.

*address correspondence to: tmanz@nmsu.edu

Abstract:

Two deactivation pathways of Ti and Zr half-metallocene complexes activated with $B(C_6F_5)_3$ in toluene solvent were studied using Density Functional Theory (DFT) with dispersion corrections: (a) H transfer from counterion to Me initiating group to release methane and (b) C_6F_5 transfer from counterion to metal. Transition state geometries and energies were computed for twenty-seven complexes, and the barrier height for the C_6F_5 transfer pathway was linearly correlated to the amount of steric congestion near the metal. Unimolecular rate constants for catalyst deactivation were predicted for all 27 catalysts by constructing a DFT-based quantitative structure activity relationship (QSAR). This QSAR was constructed by using the DFT-computed energy barrier (ΔV_0) and vibrational frequency along the reaction coordinate ($\nu^{\ddagger}$) as chemical descriptors and fitting QSAR parameters to experimental data for reference systems. The computed rate constants were in excellent agreement with available experimental data. Specifically, the dominant deactivation pathway for each catalyst and the relative deactivation rates of different catalysts were correctly predicted. Of note, the IndTi(OC_6H-2,3,5,6-Ph_4)Me_2/$B(C_6F_5)_3$ system is predicted to have a good combination of slow deactivation and high olefin polymerization rates.

keywords: single-site catalysis, homogeneous catalysis, olefin polymerization, quantitative structure activity relationships, QSARs, catalyst deactivation, half-sandwich complexes, DFT, density functional theory, reaction rate constants, kinetic modeling

1. Introduction

Studying chemical reactions is one of the primary uses of *ab initio* quantum chemistry methods like density functional theory (DFT). A common goal is to predict the relative or absolute rates of several alternate reactions. Although the reaction with lower computed barrier height is usually the preferred pathway, rate constant computation is required for a proper prediction of the preferred reaction pathway. In conventional transition state theory (CTST), the rate constant takes the form[1, 2]

$$k^{CTST} = \frac{k_B T}{h}\frac{Q^{\ddagger}}{Q_r} = \frac{k_B T}{h} e^{-\Delta G^{\ddagger}/(k_B T)}, \qquad (1)$$

where $Q^{\ddagger}$ and Q_r are the partition functions of the activated complex and reactant, T is absolute temperature, $\Delta G^{\ddagger}$ is the free energy of the transition state (TS) minus reactants, h is the Planck constant and k_B is the Boltzmann constant. The computational prediction of rate constants with CTST is difficult, because modest $\Delta G^{\ddagger}$ errors produce large rate constant errors. For reactions in solution, the difficulty of modeling solute-solvent interactions makes computational prediction of rate constants especially difficult.[3-6] For complexes with low frequency modes, the entropy portion of $\Delta G^{\ddagger}$ is difficult to model both in the gas phase and in solution.

In this article, deactivation of $[Cp'\mathbf{m}(OAr)Me]^+$ $[MeB(C_6F_5)_3]^-$ (**m** = Ti, Zr; Cp' = Cp (C_5H_5), Cp* (C_5Me_5), Ind (C_9H_7)) complexes is studied as an example. These are active catalysts for polymerizing olefins like 1-hexene in aprotic solvents such as toluene, bromobenzene, and 1,2-dichlorobenzene.[7-12] As shown in Figure 1, these catalysts are formed by activating a Cp'**m**(OAr)Me_2 precatalyst with $B(C_6F_5)_3$. Experiments showed the two main deactivation pathways for CpTi(OAr)Me_2/$B(C_6F_5)_3$ complexes are (a) H transfer from the Me group of the $[MeB(C_6F_5)_3]^-$ counterion to the Ti-bound Me group of the cation to release methane gas, and (b) C_6F_5 transfer from the counterion to Ti.[13, 14] The H transfer product Cp'**m**(OAr)$CH_2B(C_6F_5)_3$ can subsequently rearrange to form Cp'**m**(OAr)(C_6F_5)($CH_2B(C_6F_5)_2$).[13, 14] In addition to irreversible deactivation, Figure 1 also shows two reversible side reactions: (c) the double activation of catalyst that occurs when two Me groups of the precatalyst are abstracted by two $B(C_6F_5)_3$ activator molecules[15-17] and (d) the reaction of activated catalyst with precatalyst to form a complex with two metal centers.[18] Each of the reactions shown in Figure 1 occurs in a single chemical step, where a single chemical step is taken to mean a process involving the

simultaneous rearrangement of chemical bonds. Deactivation for these complexes is similar to deactivation processes in related half-metallocene complexes.[19-27] To be viable for commercial-scale use, an olefin polymerization catalyst should have both high activity and high stability.[28]

An important question is how to correlate structural features of single-site olefin polymerization catalysts to their performance. This can be done by using a combination of experiments and computations to build quantitative structure activity relationships (QSARs) that correlate catalyst performance to chemical descriptors of material properties.[7-9, 19, 29-32] When modeling catalytic processes, QSARs should preferably be constructed to predict rate constants (which should be independent of reagent concentrations) as opposed to catalyst activity or selectivity (which are highly dependent on reagent concentrations).[7-9, 29, 30]

catalyst activation:

$$Cp'\mathbf{m}(OAr)Me_2 + B(C_6F_5)_3 \rightleftarrows \left[Cp'\mathbf{m}(OAr)Me\right]^+\left[MeB(C_6F_5)_3\right]^-$$

double activation:

$$\left[Cp'\mathbf{m}(OAr)Me\right]^+\left[MeB(C_6F_5)_3\right]^- + B(C_6F_5)_3 \rightleftarrows Cp'\mathbf{m}(OAr)\left(MeB(C_6F_5)_3\right)_2$$

dimerization:

$$\left[Cp'\mathbf{m}(OAr)Me\right]^+\left[MeB(C_6F_5)_3\right]^- + Cp'\mathbf{m}(OAr)Me_2 \rightleftarrows \left[\left(Cp'\mathbf{m}(OAr)Me\right)_2 Me\right]^+\left[MeB(C_6F_5)_3\right]^-$$

deactivation by H transfer to initiating group:

$$\left[Cp'\mathbf{m}(OAr)Me\right]^+\left[MeB(C_6F_5)_3\right]^- \rightarrow CH_4 + Cp'\mathbf{m}(OAr)CH_2B(C_6F_5)_3$$

deactivation by C_6F_5 transfer to metal:

$$\left[Cp'\mathbf{m}(OAr)Me\right]^+\left[MeB(C_6F_5)_3\right]^- \rightarrow Cp'\mathbf{m}(OAr)(C_6F_5)Me + MeB(C_6F_5)_2$$

Figure 1: Catalyst activation and deactivation reactions

2. Results and Discussion

Twenty-seven catalysts were studied with DFT calculations in Gaussian 03[33] using the OLYP[34, 35] exchange-correlation functional and LANL2DZ basis sets. Solvent dielectric screening was modeled with the polarizable continuum medium (PCM) model.[36] Our reasons for choosing this level of theory are now summarized. First, the OLYP exchange-correlation functional combined with the PCM model has been shown to yield relative stabilities of different ion pair forms that are in close agreement with available experimental data for these catalysts.[9]

Second, a previous study of 18 of these systems using the OLYP exchange-correlation functional showed the LANL2DZ double zeta basis set gives ion pair separation energies in vacuum and toluene solvent that are within 1 (average) ± 1 (standard deviation) kcal/mol of those computed using the 6-311++G** triple zeta basis set with polarization and diffuse functions.[8] Due to its smaller size, the LANL2DZ basis set enables faster transition state optimizations than the 6-311++G** basis set. Geometries were optimized in vacuum to better than 0.005 Å on atom positions, and 0.0025 au on forces. For ground states, different initial conditions were explored and the lowest energy conformation was selected. Transition states were optimized by the following procedure. First, a series of geometries intermediate between reactant and product were optimized with constraints placed on bond distances involved in the reaction. After optimization, the structure with the highest energy was used as an initial guess for a subsequent quadratic synchronous transit (QST3) calculation. After QST3 optimization, frequency analysis was performed. If more than one imaginary frequency was present (subject to a computational tolerance of 30 cm^{-1}), the geometry was manually modified and subsequent geometry optimization was performed using the QST3 or TS algorithms until only one imaginary frequency was present and this mode was along the reaction coordinate.

Dispersion interactions are the attractive forces between atoms in materials caused by fluctuating dipoles and higher-order fluctuating multipole moments. Local DFT functionals such as OLYP do not include these dispersion interactions. Grimme et al.'s DFT+D3(BJ) method[37, 38] was used to compute dispersion corrections. This method combines the DFT-D3 method[39] with the Becke-Johnson damping functional[40-42]. This DFT-D3(BJ) method includes both sixth- and eighth-order two-body terms (i.e., terms proportional to R_{AB}^{-6} and R_{AB}^{-8}) and coordination number dependence, but not the ninth-order three-body terms.[39] (The D3 method may be modified to include ninth-order three-body interactions, but these are not recommended to be included by default.[37, 39]) This method requires only the atomic coordinates as input to compute a semi-empirical dispersion correction to the DFT energy. The optimized OLYP/LANL2DZ geometries were used as input and the DFT+D3(BJ) dispersion energies for each geometry are listed in the ESI†.

Catalyst numbers follow the same order as used previously[7-9] and are displayed in boldface type when referred to in the text. For catalysts with substitution on only one side of the aryloxide ligand, there are two possible conformations. The proximal (p) conformation occurs

when the substituent is located on the side closest to the metal-bound Me group, and the distal (d) conformation occurs when the substituent is located on the opposite side. For catalyst **15**, the computed rotational barrier from proximal to distal conformations is 4 (without dispersion or zero-point corrections), 3.8 (with dispersion corrections), 3.7 (with zero-point corrections), and 3.6 (with dispersion and zero-point corrections) kcal/mol.

Table 1: DFT-computed energies (kcal/mol) for CpTi(OC_6H_2-2,6-Me_2-4-Br)Me_2/$B(C_6F_5)_3$ (catalyst **1**)

	no zero-point no dispersion		with zero-point no dispersion		with zero-point with dispersion		free energy no dispersion	free energy with dispersion
	vacuum	toluene	vacuum	toluene	vacuum	toluene	vacuum	vacuum
catalyst activation barrier	8.8	10.4	7.4	9.0	11.1	12.8	6.0	9.8
catalyst activation E_{rxn}	2.5	1.4	5.1	4.0	-21.6	-22.7	21.4	-5.4
dimerization E_{rxn}	2.3	-0.8	2.9	-0.2	-4.0	-7.4	13.7	6.8
double activation E_{rxn}	22.4	27.1	23.9	28.5	-10.6	-5.9	37.7	3.2
H transfer E_{rxn}	-3.5	-3.2	-5.7	-5.3	1.9	2.2	-14.7	-7.2
H transfer barrier	29.1	28.4	26.4	25.7	21.3	20.6	26.6	21.5
C_6F_5 transfer E_{rxn}	-8.6	-8.5	-10.1	-9.9	16.0	16.1	-25.9	0.1
C_6F_5 transfer barrier	33.3	34.7	32.8	34.2	21.5	22.9	33.7	22.4

Table 1 shows DFT-computed activation barriers and E_{rxn} values for several reactions involving the CpTi(OC_6H_2-2,6-Me_2-4-Br)Me_2/$B(C_6F_5)_3$ system, where the activation barrier is the electronic energy from reactant to TS. In contrast to the large solvent effect for monomer coordination,[8] solvent dielectric screening had little effect on the computed activation barrier and E_{rxn} values for catalyst activation and deactivation. Unlike monomer coordination, the activation and deactivation pathways in Table 1 do not require ion pair separation. The computed barrier for catalyst activation (~10 kcal/mol) is low compared to the barriers for catalyst deactivation (~20–30 kcal/mol). Experimentally, the pre-catalysts are observed to activate immediately upon $B(C_6F_5)_3$ addition.[14] In experiments, $B(C_6F_5)_3$ is added in only slight excess (e.g., $B(C_6F_5)_3$ to precatalyst ratio = ~ 1.0–1.1), thereby restricting double activation to a negligible amount. NMR spectroscopy shows singly activated catalyst is the dominant species.[14] As shown in Table 1, zero-point vibration corrections had only a small effect on the energetics, while dispersion and free energy corrections had significant effects. According to the DFT+dispersion free energies, formation of the H transfer product is energetically favorable (ΔG_{rxn} = -7.2 kcal/mol) and formation of the C_6F_5 transfer product is almost energetically neutral (ΔG_{rxn} = 0.1 kcal/mol).

Catalyst dimerization is predicted to be unfavorable (ΔG_{rxn} = 6.8 kcal/mol). In summary, experiments and DFT calculations show the two most important deactivation processes for these catalysts are (a) H transfer and (b) C_6F_5 transfer.

Computed barrier heights in vacuum and $v^‡$ (in wavenumber) are shown in Table 2. Here, ΔV_0 is the energy from reactant to transition state (TS) without zero-point corrections, ΔE_0 is the zero-point corrected energy from reactant to TS, and $v^‡$ is the magnitude of the imaginary frequency along the reaction coordinate. In Table 2, the entries marked '+disp.' include dispersion corrections, while the others do not. Energy barriers in vacuum and in toluene solvent are marked 'vac.' and 'tol.', respectively. For each catalyst, the difference between ΔV_0 and ΔE_0 was small. ΔV_0 varied from 33.3 to 45.6 kcal/mol for C_6F_6 transfer but only from 27.2 to 32.6 kcal/mol for H transfer. For each reaction, $v^‡$ did not vary much from catalyst to catalyst with values of ~230 (C_6F_5 transfer) and ~1000 (H transfer) cm^{-1}. C_6F_5 transfer for catalyst **16** was the one exception with a $v^‡$ of only 98 cm^{-1}. Since they differ by only a small amount from vacuum values, ΔV_0 values in toluene solvent are given in the ESI†. Selected TS geometries are shown in Figure 2. In the C_6F_5 transfer TS, the Ti-C* distance is 2.57 (catalyst **1**) and 4.20 (catalyst **16**) Å and the C*-B distance is 2.16 (catalyst **1**) and 2.93 (catalyst **16**) Å. The much larger C_6F_5 transfer distance for **16** probably led to its much lower $v^‡$.

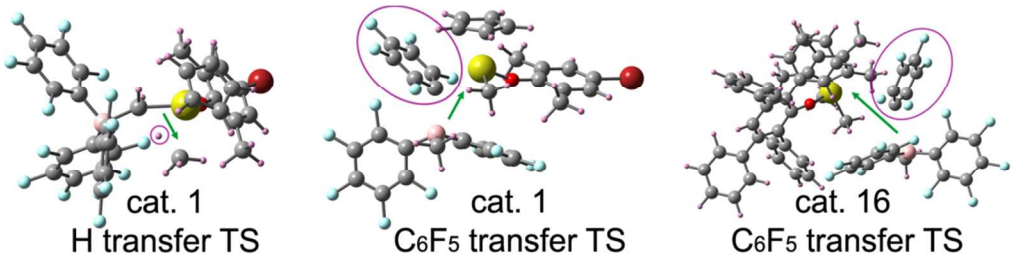

Figure 2: Selected transition state geometries (small pink = H, large pink = B, gray = C, red = O, cyan = F, yellow = Ti, large maroon = Br)

Table 2: DFT-computed transition state frequencies and energy barriers (kcal/mol) with and without dispersion corrections.

cat no.[a]	C_6F_5 transfer							H transfer						
	$v^{\ddagger}$, cm^{-1}	ΔV_0	ΔV_0 +disp.	ΔE_0	ΔE_0 +disp.	$\Delta G^{\ddagger}$	$\Delta G^{\ddagger}$ +disp.	$v^{\ddagger}$, cm^{-1}	ΔV_0	ΔV_0 +disp.	ΔE_0	ΔE_0 +disp.	$\Delta G^{\ddagger}$	$\Delta G^{\ddagger}$ +disp.
		vac.	vac.	vac.	vac.	tol.	tol.		vac.	vac.	vac.	vac.	tol.	tol.
1	199	33.3	22.1	32.8	21.6	35.0	23.7	1067	29.1	24.0	26.4	21.3	25.9	20.8
2	202	33.8	21.7	33.4	21.3	39.1	27.0	1067	29.5	25.1	26.8	22.4	29.6	25.2
3	205	34.5	23.4	33.8	22.7	37.9	26.7	1051	28.7	24.8	25.4	21.4	24.8	20.8
4	225	38.1	27.9	37.1	26.8	39.7	29.4	984	32.0	26.2	29.1	23.2	29.3	23.4
5	228	38.0	27.9	37.0	26.8	40.0	29.8	1062	30.7	25.4	27.7	22.4	36.3	31.0
6	228	38.2	28.1	37.0	26.9	39.6	29.5	900	32.0	26.3	29.3	23.6	30.1	24.4
7	220	38.0	27.6	37.0	26.6	38.1	27.7	1068	31.0	25.4	28.0	22.5	26.6	21.1
8	224	38.1	27.5	36.9	26.3	39.7	29.1	970	31.8	26.2	28.8	23.2	28.6	23.0
9	223	37.8	27.3	36.8	26.4	40.4	29.9	975	31.9	26.6	29.0	23.7	30.4	25.1
10	240	41.7	35.7	41.2	35.2	44.9	38.9	1008	29.7	24.4	27.2	21.9	29.5	24.2
11	240	42.4	37.2	41.4	36.1	42.9	37.6	964	31.9	26.9	28.4	23.4	28.6	23.6
12	237	44.7	42.9	43.6	41.9	45.8	44.1	1004	29.4	23.8	26.8	21.2	28.8	23.2
13d	240	41.4	34.2	40.4	33.3	42.9	35.7	1021	29.9	25.3	27.3	22.8	29.0	24.5
13p	238	41.7	32.9	40.6	31.8	45.3	36.5	1033	31.3	25.7	28.5	22.9	30.2	24.6
14	241	41.7	35.8	40.8	35.0	44.0	38.2	1025	29.6	24.4	27.0	21.8	29.1	23.9
15d	235	40.7	31.8	39.2	30.3	43.0	34.1	962	30.2	24.3	27.2	21.3	27.7	21.8
15p	230	39.8	29.8	38.8	28.8	42.6	32.6	876	31.4	25.9	28.9	23.4	30.9	25.4
16	98	42.3	64.1	39.1	60.9	35.8	57.5	995	27.4	19.9	24.7	17.2	26.5	19.0
17d	226	38.1	27.3	37.0	26.2	39.5	28.6	1048	30.9	25.8	28.0	23.0	28.5	23.4
17p	230	38.3	28.5	37.3	27.4	38.9	29.1	1066	30.9	25.7	28.1	22.9	27.7	22.5
18	233	38.2	28.4	37.2	27.4	41.4	31.6	912	31.8	26.3	28.7	23.2	29.4	23.9
19	214	38.2	28.3	37.2	27.3	40.7	30.8	1063	27.2	22.9	24.3	20.0	24.2	20.0
20d	233	41.2	31.8	40.1	30.6	42.5	33.0	1033	30.6	25.6	27.7	22.7	28.6	23.6
20p	230	39.8	29.9	40.9	30.9	42.8	32.9	1082	29.9	24.7	28.5	23.3	28.5	23.3
21d	240	41.9	33.4	41.1	32.7	44.1	35.7	[b]	[b]	[b]	[b]	[b]	[b]	[b]
21p	236	41.0	31.6	40.1	30.6	43.2	33.7	1056	29.8	24.2	27.2	21.6	29.4	23.7
22	229	39.7	31.1	38.4	29.8	42.6	34.0	933	32.6	23.5	29.9	20.8	34.4	25.2
23	217	36.0	25.8	35.1	24.9	37.1	26.9	1019	29.2	23.2	26.5	20.5	26.5	20.5
24	234	44.3	36.0	43.1	34.9	47.0	38.7	1063	30.6	23.8	27.8	21.0	28.1	21.2
30	241	41.9	34.8	40.6	33.5	42.8	35.6	1075	29.8	25.1	26.9	22.2	27.7	23.0
31	232	45.6	46.0	44.4	44.7	46.8	47.2	1010	29.3	24.0	26.5	21.2	28.2	23.0
33	202	33.5	22.2	33.3	22.0	38.4	27.1	1095	29.2	24.2	26.8	21.8	30.1	25.0

[a] Distal (d) or proximal (p) conformation. [b] Numerous optimizations did not show a H transfer pathway exists for the distal conformation of 21.

$\Delta G^{\ddagger}$ is the computed difference between the TS and reactant Gibbs free energies in solution. To computed these Gibbs free energies, vibrational analysis was performed on each vacuum optimized geometry and the corresponding gas phase free energy was computed in Gaussian 03 using statistical thermodynamics based on the harmonic approximation.[43, 44] Then, the free energy in solution was estimated by adding the difference between the DFT self-consistent electronic energy in toluene (PCM model) and vacuum to each gas phase free energy. All free energies reported in this paper use a standard state of 1 atmosphere pressure and a temperature of 298.15 K, which corresponds to a standard state concentration of 1 mol/22.4 L = 0.045 M for both gas and solution phase free energies. (The solution standard state is not set to 1 M, because the catalyst concentrations are typically much less than 1 M in experiments.) In previous DFT studies of these catalysts, free energies and enthalpies utilized this same standard state of 1 atmosphere pressure at 298.15 K, which corresponds to a standard state concentration of 1 mol/22.4 L = 0.045 M for both gas and solution phases.[7-9, 30]

To determine the relative importance of tunneling during H transfer, the tunneling crossover temperature, T_x, was computed:[45]

$$T_x = \frac{h\nu^{\ddagger}\Delta E_0 / k_B}{2\pi\Delta E_0 - h\nu^{\ddagger}\ln(2)}. \qquad (2)$$

Tunneling is important below T_x, but not above T_x. T_x was computed without (i.e., using 'ΔE_0' values from Table 2) and with (i.e., using 'ΔE_0+disp.' values from Table 2) dispersion corrections. As shown in Table 3, including dispersion corrections had negligible impact on T_x. As shown in Table 3, tunneling is not important for any of these systems above –18 °C. Due to the larger mass of C compared to H, tunneling is also insignificant for C_6F_5 transfer.

Table 3: DFT-computed free solid angles, tunneling crossover temperatures, and k_d values. Boldface entries denote reaction pathway (i.e., H or C_6F_5 transfer) with largest k_d for QSAR with implicit dispersion. Shaded rows mark catalysts with a predicted $k_d \leq 0.1$ hr^{-1} for QSAR with implicit dispersion.

cat no.[a]	m	Cp'	OAr substituents	Ω_f	C_6F_5 transfer to **m**				H transfer to initiating group					
					unscaled DFT		QSAR		T_x, K		k_d, hr^{-1} at 25°C			
											unscaled DFT		QSAR	
					no disp.	with disp.	implicit disp.	explicit disp.	no disp.	with disp.	no disp.	with disp.	implicit disp.	explicit disp.
1	Ti	Cp	2,6-Me_2-4-Br	2.39	5E-10	9E-02	**4E+01**	2E+01	247	248	2E-03	1E+01	4E-01	7E-01
2	Ti	Cp	2,6-Et_2	2.33	4E-13	3E-04	**2E+01**	3E+01	247	248	4E-06	8E-03	3E-01	2E-01
3	Ti	Cp	2,6-$^iPr_2$	2.01	4E-12	6E-04	**1E+01**	3E+00	244	244	1E-02	1E+01	5E-01	3E-01
4	Ti	Cp*	none	2.16	2E-13	6E-06	**5E-01**	5E-03	228	228	8E-06	1E-01	2E-02	5E-02
5	Ti	Cp*	4-F	2.13	1E-13	3E-06	**5E-01**	5E-03	246	247	5E-11	4E-07	8E-02	1E-01
6	Ti	Cp*	4-Cl	2.16	2E-13	5E-06	**5E-01**	4E-03	208	209	2E-06	3E-02	2E-02	4E-02
7	Ti	Cp*	4-Br	2.15	3E-12	1E-04	**5E-01**	7E-03	248	248	7E-04	8E+00	6E-02	1E-01
8	Ti	Cp*	4-Ph	2.15	2E-13	9E-06	**5E-01**	7E-03	225	225	2E-05	3E-01	2E-02	5E-02
9	Ti	Cp*	4-^tBu	2.16	5E-14	2E-06	**6E-01**	1E-02	226	226	1E-06	9E-03	2E-02	3E-02
10	Ti	Cp*	2,6-Me_2	1.57	3E-17	7E-13	2E-02	7E-08	234	234	5E-06	4E-02	**2E-01**	4E-01
11	Ti	Cp*	2,6-Et_2	1.51	8E-16	5E-12	9E-03	8E-09	223	224	2E-05	1E-01	**2E-02**	2E-02
12	Ti	Cp*	2,6-$^iPr_2$	1.25	6E-18	1E-16	1E-03	2E-12	233	233	2E-05	2E-01	**3E-01**	8E-01
13d	Ti	Cp*	2-cyclohexyl	1.64	8E-16	1E-10	2E-02	5E-07	237	237	1E-05	3E-02	**2E-01**	1E-01
13p	Ti	Cp*	2-cyclohexyl	1.58	1E-17	4E-11	2E-02	4E-06	239	240	2E-06	2E-02	**4E-02**	9E-02
14	Ti	Cp*	2,6-Me_2-4-Br	1.56	1E-16	2E-12	2E-02	5E-08	238	238	1E-05	6E-02	**2E-01**	4E-01
15d	Ti	Cp*	2-CH_2Ph	1.85	6E-16	2E-09	4E-02	2E-05	223	223	1E-04	2E+00	**1E-01**	4E-01
15p	Ti	Cp*	2-CH_2Ph	1.84	1E-15	3E-08	**1E-01**	3E-04	203	203	5E-07	6E-03	3E-02	6E-02
16	Ti	Cp*	2,3,5,6-Ph_4	1.05	1E-10	1E-26	4E-03	6E-26	231	232	8E-04	3E+02	**2E+00**	7E+01
17d	Ti	Cp*	3-OMe	2.17	3E-13	2E-05	**5E-01**	1E-02	243	243	3E-05	1E-01	6E-02	8E-02
17p	Ti	Cp*	3-OMe	2.17	6E-13	1E-05	**4E-01**	2E-03	247	248	1E-04	7E-01	6E-02	1E-01
18	Ti	Cp*	4-OMe	2.17	1E-14	2E-07	**5E-01**	2E-03	211	211	6E-06	6E-02	2E-02	4E-02
19	Ti	Cp	2,3,5,6-Ph_4	1.88	3E-14	5E-07	4E-01	2E-03	247	248	4E-02	5E+01	**2E+00**	2E+00
20d	Ti	Cp*	2-Br	1.79	2E-15	1E-08	3E-02	2E-05	239	240	2E-05	1E-01	**9E-02**	1E-01
20p	Ti	Cp*	2-Br	1.8	8E-16	2E-08	1E-01	3E-04	251	251	3E-05	2E-01	**2E-01**	3E-01
21d	Ti	Cp*	2-Ph	1.57	1E-16	1E-10	**2E-02**	2E-06	[b]	[b]	[b]	[b]	[b]	[b]
21p	Ti	Cp*	2-Ph	1.57	5E-16	4E-09	3E-02	2E-05	245	246	6E-06	9E-02	**2E-01**	5E-01
22	Ti	Ind	2,3,5,6-Ph_4	1.73	1E-15	3E-09	**1E-01**	5E-05	216	217	1E-09	7E-03	1E-02	1E+00
23	Ti	Ind	2,6-$^iPr_2$	1.88	1E-11	4E-04	**3E+00**	8E-02	236	237	8E-04	2E+01	3E-01	2E+00
24	Zr	Cp*	2,3,5,6-Ph_4	1.51	8E-19	9E-13	2E-03	4E-08	246	247	6E-05	6E+00	**9E-02**	9E-01
30	Ti	Cp*	2,6-$(OMe)_2$	1.74	1E-15	2E-10	1E-02	2E-07	249	250	1E-04	3E-01	**2E-01**	2E-01
31	Ti	Cp*	2,6-$^iPr_2$-4-Br	1.24	1E-18	5E-19	5E-04	3E-14	234	235	4E-05	3E-01	**3E-01**	6E-01
33	Ti	Cp	2,6-Me_2	2.44	1E-12	3E-04	**3E+01**	1E+01	254	255	2E-06	1E-02	3E-01	6E-01

[a] Distal (d) or proximal (p) conformation. [b] Numerous optimizations did not show a H transfer pathway exists for the distal conformation of **21**.

Steric congestion has a strong effect on the rate of C_6F_5 transfer.[13, 14, 21] To quantify this, the free solid angle, Ω_f, of $[Cp'\mathbf{m}(OAr)Me]^+$ $[MeB(C_6F_5)_3]^-$ was computed.[9] Ω_f equals 4π times the illuminated fraction of a spherical screen around the metal complex if a point source of light is placed at the metal's center and all portions of the complex's van der Waals surface outside the metal's van der Waals radius are made opaque.[9] As shown in Figure 3, there is a linear relationship between Ω_f and ΔV_0 for C_6F_5 transfer. With the exception of catalyst **16** mentioned

above, the linear fit had a squared correlation coefficient R^2= 0.81 without dispersion (i.e., using E_a='ΔV_0' values from Table 2) and 0.83 when dispersion corrections were included (i.e., using E_a='ΔV_0+disp' values from Table 2). Ligand cone angles are another way to quantify steric congestion in organometallic complexes. The cyclopentadienyl ligand cone angle ($\Theta_{Cp'}$) and aryloxide ligand cone angle (Θ_{OAr}) computed by the method of Manz et al.[8] are listed in Table S2 of the ESI†. The linear correlation between ΔV_0 and the ligand cone angle sum ($\Theta_{Cp'}$ + Θ_{OAr}) was weak and had a correlation coefficient R^2= 0.42. This shows the free solid angle was more strongly correlated than the ligand cone angle sum to the C_6F_5 transfer barrier heights.

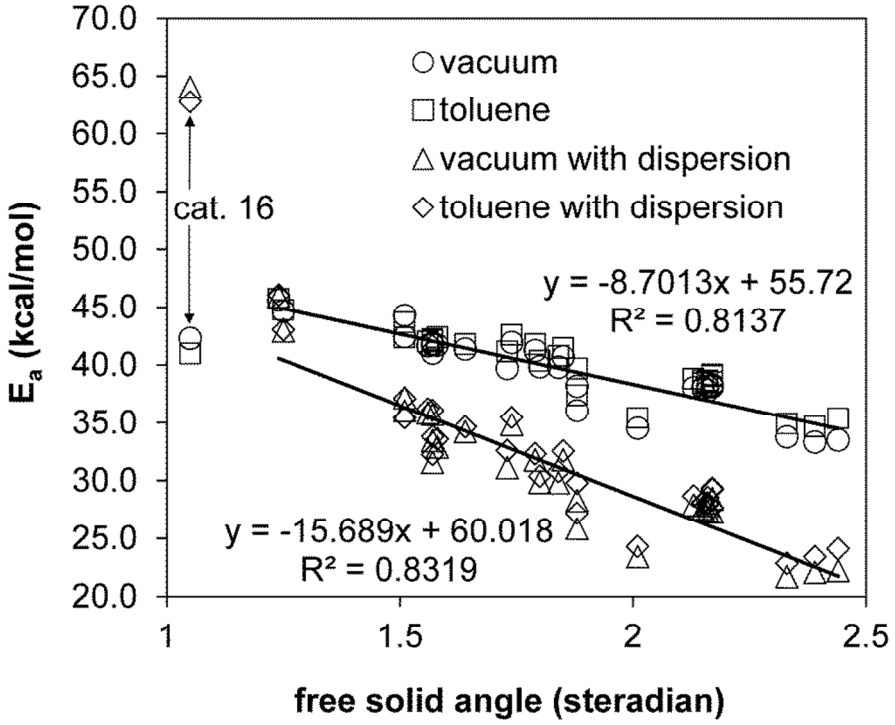

Figure 3: QSAR for the C_6F_5 transfer reaction barrier. The two lines are fit to the vacuum data (without and with dispersion corrections) excluding catalyst 16.

Catalyst deactivation rate constants (k_d) were first estimated without any adjustable parameters by inserting $\Delta G^{\ddagger}$ into (Eq. 1) using CTST. The resulting k_d values, listed in Table 3 under the columns labeled 'unscaled DFT', predict H transfer to initiating group is the dominant decay pathway for every catalyst when no dispersion corrections are included and for all catalysts except catalyst **5** when dispersion corrections are included. This prediction is wrong, because experiments show C_6F_5 transfer to metal is the dominant decay pathway for several catalysts.[13, 14] Careful examination shows the 'unscaled DFT' k_d values are erratic and span more

than 28 orders of magnitude! There are several potential sources for this discrepancy: (a) errors introduced by the solvation model (e.g., PCM), (b) errors introduced by the density functional approximation (e.g., OLYP) to the exchange-correlation energy, (c) basis set limitations, (d) errors introduced by the thermochemistry model (e.g., harmonic approximation), and (e) errors introduced by the CTST approximation itself. Of note, CTST rate constant predictions would not be exact (even for an elementary reaction) if the exact $\Delta G^{\ddagger}$ were known, because of effects like transition state recrossing.[46-49]

Repeating the calculations with alternate solvation models, exchange-correlation theories, basis sets, statistical thermochemistry models, and transition state theories would be a tedious and time-consuming process. In this article, our goal is to develop a practical model that yields accurate results with minimal effort and without redoing the DFT calculations at various levels of theory. In general, the temperature dependence of the rate constant can be approximated by the Arrhenius equation

$$k = A\exp(-E_a/(k_B T)) \qquad (3)$$

where A and E_a are approximately (but not necessarily strictly) temperature independent.[50] A QSAR for catalyst deactivation rate constants is now constructed by correlating the pre-exponential factor (A) and the effective activation energy (E_a) to DFT-computed chemical descriptors. Because the pre-exponential factor quantifies the reaction's intrinsic frequency factor, we correlated it to the imaginary frequency mode along the reaction coordinate using the model equation

$$A = c_1 \nu^{\ddagger} \qquad (4)$$

where c_1 is a fitted constant for each reaction. Because the activation energy quantifies the effective barrier height, we correlated it to the DFT-computed barrier height using the model equation

$$E_a = c_2 \times \text{barrier height} \qquad (5)$$

where c_2 is a fitted constant for each reaction.

The barrier height appearing on the right-hand side of eq. (5) could alternatively include (or not) zero-point energies, solvation effects, and/or dispersion effects. Two opposing philosophies are possible. The first philosophy, called the *Principle of Parsimony*, posits that when two competing theories explain available experiments the theory making the fewer assumptions or having a simpler mathematical form is preferable. The second philosophy posits that when two competing theories explain available experiments the theory explicitly including more interactions is preferable. At first it may appear that using a higher level of theory that explicitly includes more interactions will always produce more accurate correlations (e.g., QSARs) than a lower level of theory that explicitly includes fewer interactions, but this is not necessarily true. Including more explicit interactions comes with a trade-off. Specifically, the uncertainty in including those explicit interactions will add to the model's overall uncertainty. Thus, in cases where the uncertainty in explicitly including additional interactions (aka 'the cost') exceeds the gain in precision (aka 'the benefit'), the model will be worsened by going to a higher level of theory. On the other hand, using a lower level of theory will worsen the results if the gain in precision from explicitly including additional interactions exceeds the uncertainty costs of including those new interactions. Therefore, one cannot make universal statements of the type "higher levels of theory are better" or "lower levels of theory are better", but rather one must determine appropriate levels of theory on a case-by-case basis.

This is more subtle than it first appears, because QSARs can *implicitly* include many interactions that are not *explicitly* included. A key question when developing a QSAR is whether *implicit* or *explicit* inclusion of each interaction type is optimal. Examining Table 2, including dispersion interactions reduces the H transfer barrier heights for all catalysts and the C_6F_5 transfer barrier heights for all catalysts except catalysts **16** and **31**. This can be accounted for *explicitly* by using 'ΔV_0+disp' or 'ΔE_0+disp' as the barrier height on the right-hand side of eq. (5) . Dispersion effects can be accounted for *implicitly* by using 'ΔV_0' or 'ΔE_0' without dispersion corrections as the barrier height on the right-hand side of eq. (5) and reducing the value of parameter c_2. With the exception of a slight increase for catalyst **20p** C_6F_5 transfer, including zero-point vibrations leads to small decrease in the C_6F_5 and H transfer barrier heights. Therefore, the effects of zero-point vibrations on E_a could be modeled either (a) *explicitly* by using 'ΔE_0' or 'ΔE_0+disp' as the barrier height on the right-hand side of eq. (5) or (b) *implicitly* by using 'ΔV_0' or 'ΔV_0+disp' as the barrier height on the right-hand side of eq. (5) with an

associated decrease in c_2 compared to case (a). Including dispersion and zero-point effects implicitly in this manner is equivalent to assuming that the net effect of these interactions is proportional to the barrier height. For C_6F_5 transfer, solvation increases the barrier height by 0.6 (average) ± 0.6 (standard deviation) kcal/mol. For H transfer, solvation increases the barrier height by -0.4 (average) ± 1.1 (standard deviation) kcal/mol. Therefore, solvation does not have a significant effect on the barrier heights.

Because the zero-point and solvation effects are small in magnitude, the QSARs described below did not explicitly include them and the barrier height in vacuum without zero-point corrections was utilized. To estimate the values of c_1 and c_2 for each reaction, eqs. (3) – (5) were compared to experimental data for selected reference systems. Table 4 summarizes H transfer deactivation rates measured by Phomphrai et al. for catalyst **19**.[14] Directly fitting this experimental data gives the Arrhenius parameters $A = 7.2\times10^{11}$ hr^{-1} and $E_a = 15.7$ kcal/mol. Inserting these into eqs. (4) and (5) with the DFT-computed $v^{‡}$ and ΔV_0 for this catalyst gives $c_1 = 6.26\times10^{-6}$ (dimensionless) and $c_2 = 0.576$ (dimensionless) for the H transfer catalyst deactivation reaction. These same Arrhenius parameters were fit to eqs. (4) and (5) using 'ΔV_0+disp' as the barrier height to explicitly include dispersion corrections and generate a second model with $c_1 = 6.26\times10^{-6}$ (dimensionless) and $c_2 = 0.683$ (dimensionless). Rate constant data for a single catalyst at various temperatures is not readily available for the C_6F_5 transfer reaction. However, Phomphrai et al. reported approximate deactivation rates for catalysts **33** (-20 °C), **2** (-10 °C), **3** (10 °C),[14] which we used to estimate $c_1 = 4.63\times10^{-2}$ (dimensionless) and $c_2 = 0.55$ (dimensionless) for the C_6F_5 transfer reaction when using ΔV_0 as the barrier height in eq. (5) and $c_1 = 4.63\times10^{-2}$ (dimensionless) and $c_2 = 0.85$ (dimensionless) when using 'ΔV_0+disp' as the barrier height in eq. (5).

Table 4: Temperature dependence of the H transfer rate constant for catalysts **19**

T (°C)	experimental[a] k_d (hr^{-1})
-6	0.12
10	0.51
25	2.7
35	5.6

[a] Experimental data from reference [14].

The columns labeled 'QSAR' in Table 3 list the k_d values computed using these parameters for every catalyst. The columns marked 'implicit disp.' used ΔV_0 as the barrier

height in eq. (5) and the columns marked 'explicit disp.' used 'ΔV_0+disp' as the barrier height in eq. (5). As discussed above, the implicit dispersion models had smaller c_2 values (than the explicit dispersion models) to implicitly correct the barrier heights for dispersion. The explicit dispersion QSAR is ill-behaved for the C_6F_5 transfer reaction, because it (a) predicts the k_d values span more than 26 orders of magnitude which is too large a range and (b) incorrectly predicts the more sterically hindered catalyst **2** has a higher C_6F_5 transfer rate than the less sterically hindered catalyst **33**. These discrepancies can be attributed to uncertainties associated with constructing DFT+dispersion exchange-correlation functionals, which is intrinsically challenging owing to the need to correctly damp the add-on dispersion correction at close distances to avoid double-counting electron correlations[37, 39].

For each catalyst, the pathway with largest k_d for the implicit dispersion QSAR is shown in boldface type. Steric congestion was the main determinant of the dominant pathway. Using the implicit dispersion QSAR, all twelve catalysts with $\Omega_f > 2.0$ are predicted to decay by C_6F_5 transfer, and all nine catalysts with $\Omega_f < 1.7$ are predicted to decay by H transfer. Comparisons to experimental data can be made as follows. Phomphrai *et al.* report that the deactivation rates for **33**, **2**, **3**, and **19** are similar at -20, -10, 10, and 30 °C, respectively, where **33**, **2**, and **3** decay by C_6F_5 transfer and **19** decays by H transfer.[14] The implicit dispersion QSAR predicts the correct decay pathway for each of these catalysts, and the computed k_d values at 25 °C follow the same trend in deactivation rates: **33** (31 hr^{-1}) > **2** (24 hr^{-1}) > **3** (12 hr^{-1}) > **19** (2 hr^{-1}). Experiments show **12** decomposes by H transfer,[10] the same pathway our calculations predict. The implicit dispersion QSAR predicts catalysts **11**, **15**, **22**, and **24** to be the most stable with a predicted $k_d \leq$ 0.1 hr^{-1} at 25 °C. Using the implicit dispersion QSAR as the lower bound on k_d and the explicit dispersion QSAR as the upper bound on k_d leads to the predictions k_d = 0.02 (cat. **11**), 0.1–0.4 (cat. **15**), 0.1–1.0 (cat. **22**), and 0.09–0.9 (cat. **24**) hr^{-1}. Catalysts **20** and **22** were previously found to have the highest olefin polymerization rates of all catalysts in Table 3 and exhibit opportunistic ligand coordination that lowers the ion pair separation energy to facilitate monomer coordination.[8] Catalyst **22** is also highly desirable because it can be purified by crystallization during synthesis and gives facile chain initiation during olefin polymerization.[8, 9]

3. Conclusions

In summary, density functional theory was used to study $[Cp'\mathbf{m}(OAr)Me]^{+}[MeB(C_6F_5)_3]^{-}$ deactivation by two different pathways. The barrier height for C_6F_5 transfer was found to linearly increase as steric congestion at the metal increased, and tunneling was found to be unimportant for both pathways. Quantitative structure activity relationships (QSARs) were constructed to estimate each deactivation rate constant from the DFT-computed energy barrier and vibrational frequency along the reaction coordinate. This method of using *ab initio* calculations coupled with experimental reference data to construct QSARs for estimating rate constants should find widespread applications to related processes. For each catalyst whose deactivation mechanism had been experimentally determined, the rate constants estimated with the implicit dispersion QSAR correctly predicted which decay pathway is dominant and the relative stabilities of different catalysts. Computations identified catalyst **22** with low deactivation rates that is known to have high olefin polymerization rates, and this catalyst would be a good candidate for follow-up studies investigating counterion, solvent, or monomer variations.

A detailed analysis of dispersion, zero-point, and solvation energies showed including these in the QSAR *implicitly* was more expedient than including them in the QSAR *explicitly* for these particular reactions. This illustrates the general principle that models explicitly including more interactions (aka 'higher levels of theory') are better if and only if the additional uncertainty associated with explicitly including these new interactions is outweighed by an increase in precision when the new interactions are explicitly included.

Acknowledgements

Computational resources were provided by the Teragrid Network, Purdue University, and the Extreme Science and Engineering Discovery Environment (XSEDE). Thanks to Dr. James Caruthers and Dr. Kendall Thomson, my former Ph.D. advisors, for introducing me to the subject of building QSARs for single-site olefin polymerization catalysts, which provided some of the motivation for this work.

† **Electronic Supplementary Information (ESI) available**: Optimized geometries, energies in vacuum and toluene, ligand cone angles, and frequencies for reactants, transition states, and products.

References

1. R. Hernandez and W. H. Miller, *Chem. Phys. Lett.*, 1993, **214**, 129-136.
2. K. J. Laidler and M. C. King, *J. Phys. Chem.*, 1983, **87**, 2657-2664.
3. J. N. Harvey, *Faraday Discuss.*, 2010, **145**, 487-505.
4. R. Hernandez, T. Uzer and T. Bartsch, *Chem. Phys.*, 2010, **370**, 270-276.
5. D. G. Truhlar, B. C. Garrett and S. J. Klippenstein, *J. Phys. Chem.*, 1996, **100**, 12771-12800.
6. H. Azzouz and D. Borgis, *J. Chem. Phys.*, 1993, **98**, 7361-7375.
7. T. A. Manz, K. Phomphrai, G. Medvedev, B. B. Krishnamurthy, S. Sharma, J. Haq, K. A. Novstrup, K. T. Thomson, W. N. Delgass, J. M. Caruthers and M. M. Abu-Omar, *J. Am. Chem. Soc.*, 2007, **129**, 3776-3777.
8. T. A. Manz, S. Sharma, K. Phomphrai, K. A. Novstrup, A. E. Fenwick, P. E. Fanwick, G. A. Medvedev, M. M. Abu-Omar, W. N. Delgass, K. T. Thomson and J. M. Caruthers, *Organometallics*, 2008, **27**, 5504-5520.
9. T. A. Manz, J. M. Caruthers, S. Sharma, K. Phomphrai, K. T. Thomson, W. N. Delgass and M. M. Abu-Omar, *Organometallics*, 2012, **31**, 602-618.
10. K. Nomura and A. Fudo, *Inorg. Chim. Acta*, 2003, **345**, 37-43.
11. K. Nomura, *Dalton Trans.*, 2009, 8811-8823.
12. K. Nomura and J. Liu, *Dalton Trans.*, 2011, **40**, 7666-7682.
13. A. E. Fenwick, K. Phomphrai, M. G. Thorn, J. S. Vilardo, C. A. Trefun, B. Hanna, P. E. Fanwick and I. P. Rothwell, *Organometallics*, 2004, **23**, 2146-2156.
14. K. Phomphrai, A. E. Fenwick, S. Sharma, P. E. Fanwick, J. M. Caruthers, W. N. Delgass, M. M. Abu-Omar and I. P. Rothwell, *Organometallics*, 2006, **25**, 214-220.
15. A. Al-Humydi, J. C. Garrison, W. J. Youngs and S. Collins, *Organometallics*, 2005, **24**, 193-196.
16. D. W. Stephan, *Macromol. Symp.*, 2001, **173**, 105-115.
17. D. W. Stephan, *Organometallics*, 2005, **24**, 2548-2560.
18. M. Bochmann and S. J. Lancaster, *Angew. Chem. Int. Ed.*, 1994, **33**, 1634-1637.
19. E. Y. X. Chen and T. J. Marks, *Chem. Rev.*, 2000, **100**, 1391-1434.
20. V. Tabernero, C. Maestre, G. Jimenez, T. Cuenca and C. R. de Arellano, *Organometallics*, 2006, **25**, 1723-1727.
21. T. Wondimagegn, Z. T. Xu, K. Vanka and T. Ziegler, *Organometallics*, 2004, **23**, 3847-3852.
22. T. Wondimagegn, K. Vanka, Z. T. Xu and T. Ziegler, *Organometallics*, 2004, **23**, 5737-5743.
23. T. Wondimagegn, K. Vanka, Z. T. Xu and T. Ziegler, *Organometallics*, 2004, **23**, 2651-2657.
24. T. Wondimagegn, Z. T. Xu, K. Vanka and T. Ziegler, *Organometallics*, 2005, **24**, 2076-2085.
25. N. Yue, E. Hollink, F. Guerin and D. W. Stephan, *Organometallics*, 2001, **20**, 4424-4433.
26. S. Zhang, W. E. Piers, X. L. Gao and M. Parvez, *J. Am. Chem. Soc.*, 2000, **122**, 5499-5509.
27. T. A. Manz, A. E. Fenwick, K. Phomphrai, I. P. Rothwell and K. T. Thomson, *Dalton Trans.*, 2005, 668-674.

28. P. M. Gurubasavaraj, H. W. Roesky, B. Nekoueishahraki, A. Pal and R. Herbst-Irmer, *Inorg. Chem.*, 2008, **47**, 5324-5331.
29. J. M. Caruthers, J. A. Lauterbach, K. T. Thomson, V. Venkatasubramanian, C. M. Snively, A. Bhan, S. Katare and G. Oskarsdottir, *J. Catal.*, 2003, **216**, 98-109.
30. T. A. Manz, *QSARs for Olefin Polymerization Catalyzed by Ti and Zr Complexes*, Scholars' Press, Saarbrucken, Germany, 2013 (ISBN 978-3-639-51617-3).
31. V. L. Cruz, J. Ramos, S. Martinez, A. Munoz-Escalona and J. Martinez-Salazar, *Organometallics*, 2005, **24**, 5095-5102.
32. V. L. Cruz, S. Martinez, J. Ramos and J. Martinez-Salazar, *Organometallics*, 2014, **33**, 2944-2959.
33. M. J. Frisch, G. W. Trucks, H. B. Schlegel, G. E. Scuseria, M. A. Robb, J. R. Cheeseman, J. Montgomery, T. Vreven, K. N. Kudin, J. C. Burant, J. M. Millam, S. S. Iyengar, J. Tomasi, V. Barone, B. Mennucci, M. Cossi, G. Scalmani, N. Rega, G. A. Petersson, H. Nakatsuji, M. Hada, M. Ehara, K. Toyota, R. Fukuda, J. Hasegawa, M. Ishida, T. Nakajima, Y. Honda, O. Kitao, H. Nakai, M. Klene, X. Li, J. E. Knox, H. P. Hratchian, J. B. Cross, C. Adamo, J. Jaramillo, R. Gomperts, R. E. Stratmann, O. Yazyev, A. J. Austin, R. Cammi, C. Pomelli, J. W. Ochterski, P. Y. Ayala, K. Morokuma, G. A. Voth, P. Salvador, J. J. Dannenberg, V. G. Zakrzewski, S. Dapprich, A. D. Daniels, M. C. Strain, O. Farkas, D. K. Malick, A. D. Rabuck, K. Raghavachari, J. B. Foresman, J. V. Ortiz, Q. Cui, A. G. Baboul, S. Clifford, J. Cioslowski, B. B. Stefanov, G. Liu, A. Liashenko, P. Piskorz, I. Komaromi, R. L. Martin, D. J. Fox, T. Keith, M. A. Al-Laham, C. Y. Peng, A. Nanayakkara, M. Challacombe, P. M. W. Gill, B. Johnson, W. Chen, M. W. Wong, C. Gonzalez and J. A. Pople, *GAUSSIAN 03*, 2003.
34. N. C. Handy and A. J. Cohen, *Mol. Phys.*, 2001, **99**, 403-412.
35. W. M. Hoe, A. J. Cohen and N. C. Handy, *Chem. Phys. Lett.*, 2001, **341**, 319-328.
36. M. Cossi, V. Barone, R. Cammi and J. Tomasi, *Chem. Phys. Lett.*, 1996, **255**, 327-335.
37. S. Grimme, S. Ehrlich and L. Goerigk, *J. Comput. Chem.*, 2011, **32**, 1456-1465.
38. S. Grimme, DFT-D3 Program Version 3.1 Revision 0, June 20, 2014, http://www.thch.uni-bonn.de/tc/index.php?section=downloads&subsection=DFT-D3&lang=english, (accessed March 2015).
39. S. Grimme, J. Antony, S. Ehrlich and H. Krieg, *J. Chem. Phys.*, 2010, **132**,154104.
40. A. D. Becke and E. R. Johnson, *J. Chem. Phys*, 2005, **122,** 154104.
41. A. D. Becke and E. R. Johnson, *J. Chem. Phys*, 2005, **123,** 154101.
42. E. R. Johnson and A. D. Becke, *J. Chem. Phys*, 2006, **124,** 174104.
43. D. A. McQuarrie and J. D. Simon, *Molecular Thermodynamics*, University Science Books, Sausalito, CA, 1999.
44. J. W. Ochterski, Thermochemistry in Gaussian, April 19, 2000, http://www.gaussian.com/g_whitepap/thermo.htm, (accessed April 2015).
45. J. T. Fermann and S. Auerbach, *J. Chem. Phys.*, 2000, **112**, 6787-6794.
46. D. G. Truhlar, B. C. Garrett, P. G. Hipes and A. Kuppermann, *J. Chem. Phys.*, 1984, **81**, 3542-3545.
47. J. Rehbein and B. K. Carpenter, *Phys. Chem. Chem. Phys.*, 2011, **13**, 20906-20922.
48. Y. Oyola and D. A. Singleton, *J. Am. Chem. Soc.*, 2009, **131**, 3130-3131.
49. J. R. E. T. Pineda and S. D. Schwartz, *Phil. Trans. R. Soc. B*, 2006, **361**, 1433-1438.
50. S. Arrhenius, *J. Phys. Chem.*, 1889, **4**, 226.